DAMAGE TOLERANCE EVALUATION OF WING BOTTOM SKIN PANEL OF AN AIRCRAFT

Nagesh R. Iyer*, A. Rama Chandra Murthy*, J. Rajasankar* and G.S. Palani*

Abstract

This paper presents the details of damage tolerance evaluation of a Wing Bottom Skin Panel (WBSP) of an aircraft. Finite element analysis (FEA) of an integrally stiffened WBSP has been conducted to identify the probable location for crack initiation and the same has been confirmed by conducting experiments. Linear elastic fracture mechanics (LEFM) principles have been used for computation of stress intensity factor (SIF). Static results obtained from FEA and experiments are found to compare well. SIF has been computed for different crack lengths in mode I under intact-stiffener condition by using displacement extrapolation and strain energy release rate (SERR) techniques. SIF has also been computed for the same crack lengths under broken stiffener and unstiffened conditions. A comparison between the residual strength predicted under intact-stiffener, broken stiffener and unstiffened conditions clearly indicates the efficacy of the stiffener in arresting the crack propagation.

***Key Words**: Aircraft, Wing bottom skin panel, Finite element method, Stress intensity factor, Residual strength, damage tolerance*

Nomenclature

a	= crack length
e	= eccentricity
f_{ij}	= function of θ
j	= safety factor
K	= stress intensity factor
P	= applied load
P_{max}	= maximum load
P_{res}	= residual strength
P_s	= service load
P_u	= ultimate strength
R	= radius of circular hole
S_x	= nodal stress
t	= thickness
u_x	= in-plane displacement
u_z	= out-of-plane displacement
W	= width
β,β_1,β_2	= geometric correction factors
r,θ	= polar co-ordinate system
θ_y	= longitudinal rotation
σ_{fc}	= nominal stress
σ	= applied far-field stress
σ_{ij}	= stress in the vicinity of the crack tip
σ_x	= contour of stress along x-direction
σ_y	= yield stress
ξ	= aspect ratio = $\frac{a}{R}$
ΔK	= stress intensity factor range
$\Delta\sigma$	= applied stress range

Introduction

Aircraft structure is one where functional requirements demand light weight and, therefore, most of the structural components are expected to withstand high operating stresses. An efficient structural element must have three primary attributes; namely, the ability to perform its intended function, adequate service life, and the capability of being produced at reasonable cost. To ensure the safety of aircraft structures, aviation regulations require damage tolerance design of critical structural components. Stiffened structural components like wing and fuselage are critical components of an aircraft. Cracks may occur in these structural components near the stress concentration regions during flight operations. A structural component is considered damage tolerant if it can sustain operating loads in the presence of cracks safely until it is detected and repaired. Damage tolerance analysis provides infor-

* Scientists, Structural Engineering Research Centre, Taramani, Chennai-600 113, India, Email : nriyer@sercm.csir.res.in
Manuscript received on 03 Sep 2004; Paper reviewed, revised and accepted on 26 Jul 2005

mation about the effect of cracks on the strength of the component/structure. This information is usually presented in the form of two diagrams, namely, the residual strength diagram and the crack growth diagram. From the residual strength diagram, it is possible to predict the maximum crack length that can be sustained safely. This data is used in the crack growth diagram to find the number of loading cycles that will be required for the crack to grow to its critical length.

During the last four decades, a great deal of research has been carried out on the computation of SIF in cracked stiffened panels. Configurations having cracks in infinite sheets, subjected to uniaxial stresses, reinforced with continuously attached (bonded or integral) or discretely attached (riveted) stiffeners have been studied by several authors [1,2,3]. However, engineering structures can have complex shapes and cracks tend to occur in regions of high stress concentration, such as corners, cut-outs and edges. Hence, it is important to consider all the above aspects in order to predict the stress concentration region for crack initiation study and damage tolerance evaluation. Fracture mechanics is used as a tool to conduct damage tolerance analysis. It provides the concepts and related equations to estimate crack driving force and remaining strength of a structure. FEM has been extensively used for the analysis of cracked structural components. Practically, for all the materials used in the aerospace industry, damage tolerance analysis can be performed using LEFM principles, in which case, SIF is an important fracture mechanics parameter.

Toor [4] conducted an extensive review on damage tolerant design approaches for aircraft structures. It is pointed out that the residual strength analysis methodology, crack propagation laws and fracture mechanics can be applied to evaluate damage tolerance capacity of built-up structural components under spectrum loading conditions. The results of the test and finite element analysis (FEA) of complex structures indicated that simple methods of fracture mechanics can be applied to find the degree of damage tolerance. Woods [5] discussed the significant factors leading to the development of damage tolerance criteria and illustrated the role of fracture mechanics in the analysis and testing aspects necessary to satisfy these requirements. Brussat et al.[6] presented the details of damage tolerance assessment of aircraft attachment lugs. Toor and Dagger [7,8] explained the details of damage tolerant design of fuselage structures with longitudinal cracks and circumferential cracks. Swift [9] conducted fracture analysis of cracked stiffened structure based on displacement compatibility method. Residual strength was computed considering a two bay skin crack with a broken stiffener condition. Roudolff and Gadre [10] studied the damage tolerance of composite structures for large transport aircraft.

This paper presents details of damage tolerance evaluation of WBSP through FE modelling strategy and procedures for crack growth analysis of the WBSP subjected to in-plane tensile loading. Static analysis of WBSP has been conducted by using FEM. Static test has been conducted on WBSP and the results have been compared with those of FEA. Fatigue crack has been modelled at the point of maximum stress location (Fig.12) towards the cut-out free surface and later towards the integral stiffener. LEFM principles have been used for computation of SIF. For different crack lengths, SIF for mode I under intact-stiffener condition has been computed by using displacement extrapolation technique and compared with those obtained by using SERR technique. It is observed that SIF increases with crack length upto certain point and then begins to drop as the crack tip approaches an intact-stiffener. SIF reaches a minimum value for the crack tip just after the stiffener location and then begins to increase again with crack length. Residual strength has been calculated by making use of SIF values. Studies have also been conducted for the broken-stiffener condition and unstiffened condition and the corresponding SIFs and residual strengths have been evaluated. From the studies, it is observed that under intact-stiffener condition the stiffener can arrest the crack up to a considerable amount of design stress compared to unstiffened condition.

FE Modelling and Static Analysis

FE Modelling

Accurate determination of SIF for a structure with complex geometry such as stiffened plate shell/panels with cut-outs requires detailed and accurate modelling of the components. The accuracy of SIF computed by using the results of FEA to a large extent depends on the FE model employed in the studies. A large number of FE models and formulations can be employed in the analysis [11]. These may be represented by facet plate/shell elements, thin-shell formulation (Kirchoff theory), thin/thick shell formulation (Reissner-Mindlin theory) and three dimensional elements. The choice of an element for analysis depends on the geometry of the structure and the purpose for which the results of the analysis is being used. Shell elements are generally preferred to model plate/shell panels. For an economical analysis, FE modelling techniques

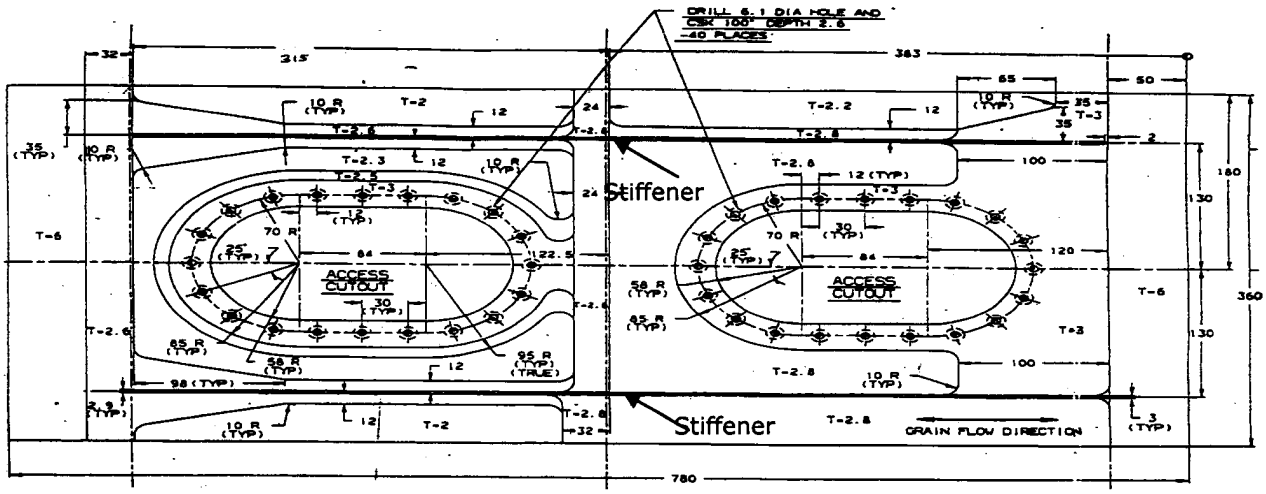

Fig. 1 Geometry details of WBSP

Table-1 : Material properties

Component/Location	Material	Young's Modulus (MPa)	Poisson's Ratio	Yield Strength (MPa)	Ultimate Strength (MPa)
Clamp and bolts (Fixtures)	Steel	2×10^5	0.3	344.5	485.2
Base plate and stiffeners	2024-T3 Aluminium Alloy	7.5×10^4	0.3	372.1	463.8
Between plate and clamp	Gap	0.1	0.1	0.1	0.1

should be suitably chosen to reduce the problem size without loss of significant accuracy in the result. In the stress concentration regions finer mesh should be employed in order to capture the response of the structure/structural component. Another important aspect of modelling is, crack lengths are to be modelled by separating the elements at the nodal points along the crack line. In order to compute SIF accurately, one can use crack tip singular elements.

WBSP is one of the critical components of an aircraft (Fig.1). In the present study WBSP is idealized as a rectangular plate with variable thicknesses built-in on one side (inner side) so that the other surface (outer side) remains smooth to satisfy aerodynamic requirements. The edges of the large cut-outs are stiffened by thickening. Auxiliary holes are provided all around the cut-outs to fasten cover plates. Some of these auxiliary holes form fatigue critical locations in the panel. The plate is provided with a stiffener on either side of the cut-outs running

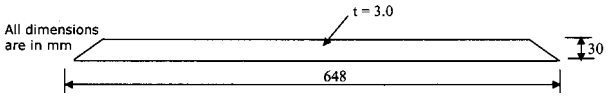

Fig. 2 Geometry details of stiffener

longitudinally. The material of the plate and stiffener are 2024-T3 aluminium alloy. Geometry details of typical WBSP and stiffener are shown in Figs.1 and 2 respectively. In order to corroborate the analytical/numerical results with those of the, experimental tests conducted on a model in the laboratory, clamps are also modelled. Fig. 3 shows the cross section details at the clamp location. Material properties of WBSP are shown in Table-1. There are twenty auxiliary holes around each cut-out as shown in Fig.1. Diameter of each auxiliary hole through the thickness of the panel decreases gradually from inner side to outer side as shown in Fig.4, due to countersinking.

FE model has been created as per the dimensions shown in Figs.1 to 4. At the clamp location (Fig. 3), there

are two materials joined together i.e. base plate - aluminium alloy and clamp - steel. It is obvious that there exists some gap between steel and aluminium when they are placed together. The gap between steel and aluminium is modelled as plate elements prescribed by assuming very low value of modulus of elasticity. This is necessary and important in order to reduce the inter laminar shear stresses that will be developed when WBSP is subjected to in-plane tensile loading. The bolt holes provided in the clamp are also considered in the modelling. To represent the variation of the diameter of auxiliary holes through thickness in the FE modelling, the holes are modelled by considering quadratic variation of thickness from one side to other side. From Fig.1, it is observed that one can expect, stress concentration near some of the auxiliary holes where geometry changes from elliptical to rectangular shape around the cut-out portion. Finer meshing is employed at these selected regions in order to capture the response of the component. For accurate representation of steel and aluminium at the clamp location and thickness variation in WBSP, layered shell element is the best option for the base plate and general shell element for the stiffener. FEA software ANSYS [12] and its associated modules have been used for modelling as well as for analyses. To represent the thickness variation in the plate, different areas have been created corresponding to each different thickness. In the present study, linear layered 8-noded shell element (shell 99) is used to represent the base plate and general 8-noded shell element (shell 93) is used to model the stiffeners [13]. Both the elements have six degree of freedoms (three translation and three rotations) at each node. FE idealization of WBSP and a zoomed view of the mesh near the rivet holes are shown in Figs. 5(a) and 5(b) respectively along with the salient details of FE mesh used for analysis. An in-plane uniform tensile loading of 20 KN is applied as work equivalent load distributed on all the nodes along the outward edge of the right clamp. Out-of-plane displacement, U_z and longitudinal rotation, θ_y corresponding to these nodes are arrested. All DoF of the nodes along the left end of the clamp are arrested to simulate the fixity condition of the experimental set-up.

Static Analysis

Linear static analysis of WBSP is carried out using the FE model described above. In- plane displacement (U_x) contour is shown in Fig. 6. Fig. 7 shows the variation of out-of-plane displacement (U_z) along the length of the plate. The out-of-plane deformation is due to the eccentricity of the load as shown in Fig. 8. It is observed that the maximum out-of-plane displacement is 0.97 mm which is

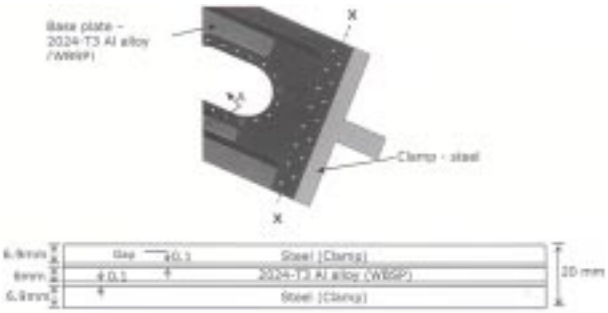

Fig. 3 Details of section at XX

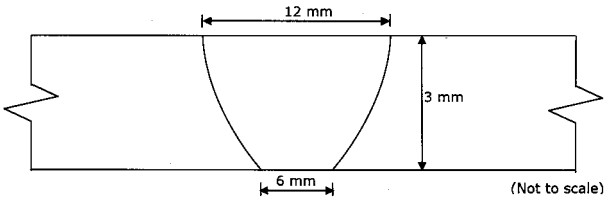

Fig. 4 Sectional view of an auxiliary hole (Section A-A corresponding to Fig. 3)

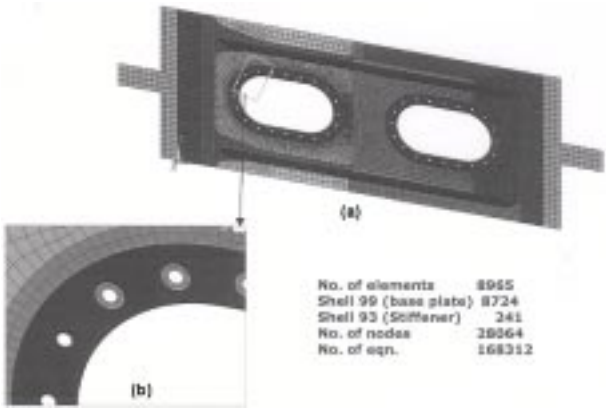

Fig. 5 (a) FE idealization
(b) Zoomed view of FE idealization near the rivet holes

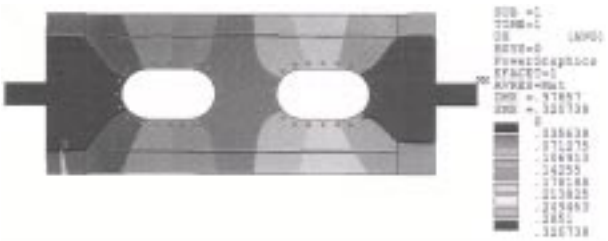

Fig. 6 In-plane displacement (u_x) contour

less than the minimum thickness of the plate and hence it is assumed that it will not cause any non-linearity. Plot of contour of stress (σ_x) is presented in Fig. 9. Further, it is observed that the maximum tensile stress occurs at one of the auxiliary holes around the cut-out as indicated in Fig. 9.

Experimental Studies

Experimental studies were conducted on WBSP model for the same loading condition as in the case of FEA. Fig. 10 shows WBSP specimen with strain gage instrumentation. Static test on WBSP is conducted using computer controlled universal testing machine of capacity ±500 kN. Total load is applied incrementally. For each incremental load, strains are measured using data acquisition system.

The corresponding stresses are calculated for the strains obtained experimentally based on uniaxial stress distribution in the plate. Table-2 shows the location of strain gages, the derived stress from the measured strain and also the nearest FE node with its coordinates and the corresponding nodal stress. From Table-2, it can be observed that there is a difference of about 20-25% of nodal stresses at some locations obtained by FEA and experiments. It is generally expected that there will be difference between analytical and experimental observations. And it also known that this difference is problem dependent. For the present problem, a refined mesh has been employed near the stress concentration region (steep strain gradient) where a small change in the location will lead to large difference in the results between FEA and experiment. One of the reasons for the large difference at few locations is attributed to non-coincident of strain gauge location and finite element node location which is very vital.

SIF Computation

SIF, which is an important parameter for the damage tolerance evaluation of structural components, can be computed by using LEFM principles. Irwin [14] used the classical theory of elasticity to show that the stresses in the vicinity of the crack tip are of the form

$$\sigma_{ij} \infty \frac{1}{\sqrt{2\pi r}} f_{ij}(\theta) + \ldots \quad (1)$$

where r and θ form polar co-ordinate system with its origin at the crack tip, as shown in Fig.11 and f_{ij} is a function of θ.

Fig. 7 Out-of-plane displacement (u_z) contour

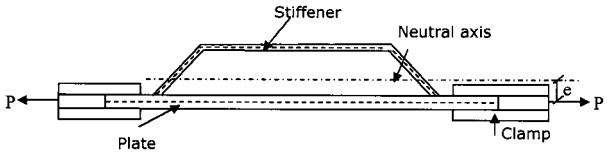

Fig. 8 Cross-section of plate with stiffener

Fig. 9 σ_x - stress contour

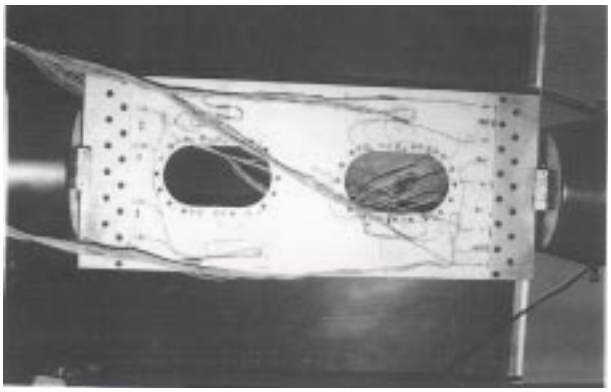

Fig. 10 WBSP with strain gage instrumentation

This equation can be written as

$$\sigma_{ij} = \frac{K}{\sqrt{2\pi r}} f_{ij}(\theta) + \ldots \quad (2)$$

where,

$$K = \beta\sigma\sqrt{\pi a} \quad (3)$$

Table-2 : Comparison of results of static analysis with experimental results

Strain gage ID	Coordinates, mm (from analysis)		Nodal stress (S_x), MPa (analysis)$^+$	Coordinates at strain gage location, mm		Derived stress based on measured strain, MPa
	X	Y		X	Y	
1(NS)*	627.67	239.99	45.15	628	240	53.1
2(NS	567.99	240.16	38.12	567	240	39.6
3(NS)	505.01	239.00	35.9	504	240	43.0
4(NS)	625.93	121.85	45.5	628	121.5	55.6
5(NS)	568	122.0	35.8	567	121.5	41.2
6(NS)	506.36	121.69	36.17	504	121.5	44.5
8(NS)	290.22	239.27	44.0	291	240	44.9
9(NS)	232.49	240.16	41.0	233	240	45.4
10(NS)	172.5	239.98	50.7	172	240	64.1
12(NS)	232.5	122	39.1	233	121.5	45.7
14	628.27	240.38	45.6	628	240	39.8
16	567.99	244.63	48.8	567	244	39.6
17	567.99	240.16	33.9	567	240	27.9
18	505.01	239	30.0	504	240	28.8
19	625.93	121.85	45.9	628	121.5	45.8
20	568	122	31.7	567	120.5	26.4
21	567.05	115.41	48.2	567	115.5	34.3
23	506.36	121.69	30.4	504	121.5	27.3
25	291.69	240.56	35.17	291	240	30
27	232.49	244.63	52.1	233	244	40.5
28	232.49	240.16	36	233	240	28.7
29	172.2	239.23	48.5	172	240	48.6
30	292.47	120.18	32.8	293	121.5	31.1
31	232.5	122.0	34.2	233	120.5	26.1
33	234.08	105.01	50.5	233	105.5	38.4
34	171.39	120.92	46.7	173	121.5	45.7
35	71.33	310	44.4	70	310	44.4
36	71.33	50	44.2	70	49	39.9
44(NS)	66.0	227.5	11.85	65	227	16.1
45(NS)	66.0	132.5	11.87	65	131.5	16.6
46(NS)	60.667	58.75	15.39	65	56	19.0
1A(NS)	66	327.5	10.7	65	333	8.6
2A(NS)	66	265.5	14.5	65	264.5	13.6
3A(NS)	66	180	7.12	65	176.5	9.9

Table-2 (Contd) : Comparison of results of static analysis with experimental results

Strain gage ID	Coordinates, mm (from analysis)		Nodal stress (S_x), MPa (analysis)$^+$	Coordinates at strain gage location, mm		Derived stress based on measured strain, MPa
	X	Y		X	Y	
4A(NS)	66	94.5	14.6	65	91	19.7
5A(NS)	60.667	23.75	9.84	65	27	9.1
6A	71.33	345	31.9	70	340	31.9
7A	71.33	256	31.14	70	257	34.6
8A	71.33	218.0	23.15	70	216	20.8
9A	71.33	165.75	18.69	70	168	14.1
10A	71.33	118.25	28.4	70	118	26.0
11A	71.33	85	34.88	70	85	34.8
12A	71.33	23.75	36.28	70	19	28.5

** NS - Non-stiffened side* $^+$ *- Not necessarily at exact strain gage locations, but close to it*

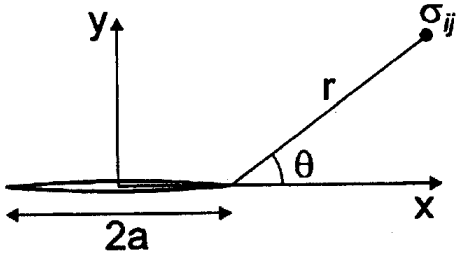

Fig. 11 Co-ordinate system for crack tip

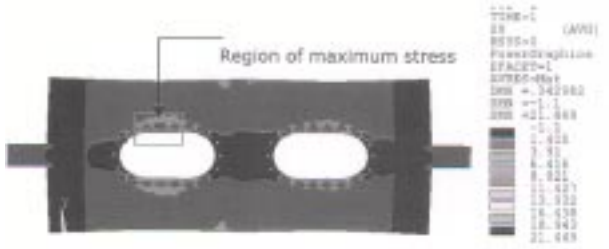

Fig. 12 σ_x - stress contour

In eqn. (3), β is a geometric correction factor and σ is the applied far-field stress. In the context of a stiffened plate, β-factor must account for the plate configuration, global and local geometries, loading mode, crack shape and position.

SIF range (Δ*K*)for the cyclic applied stress range (Δσ) can be calculated from eqn. (3)

$$\Delta K = \beta \Delta\sigma \sqrt{\pi a} \tag{4}$$

In order to validate the displacement extrapolation technique adopted for SIF computation of WBSP, static analysis has been conducted for WBSP without stiffeners. From the analysis, it is observed that the maximum stress occurs at the same location/region as in the case of WBSP with stiffeners. Fig. 12 shows that the σ_x stress contour and location of maximum stress. Fatigue crack is assumed to initiate at the point of maximum tensile stress location and propagates towards the other end. Geometry factor was calculated for different crack lengths and compared with those obtained for a plate having circular hole at the centre and a single crack emanating from the hole [15]. Geometric factor (β) is computed by using the following equation (15).

$$\beta = \beta_1 . \beta_2 \tag{5}$$

where,

$$\beta_1 = \sqrt{(2+\xi)/(2+2\xi)} \cdot \left[1 + \frac{0.2\xi}{(1+\xi)^3}\right] \tag{6}$$

$$\beta_2 = 1 + \frac{1}{(2\xi^2 + 1.93\xi + 0.539)} + \frac{1}{2(\xi+1)} \tag{7}$$

$\xi = \frac{a}{R}$, a = crack length, R = radius of circular hole.

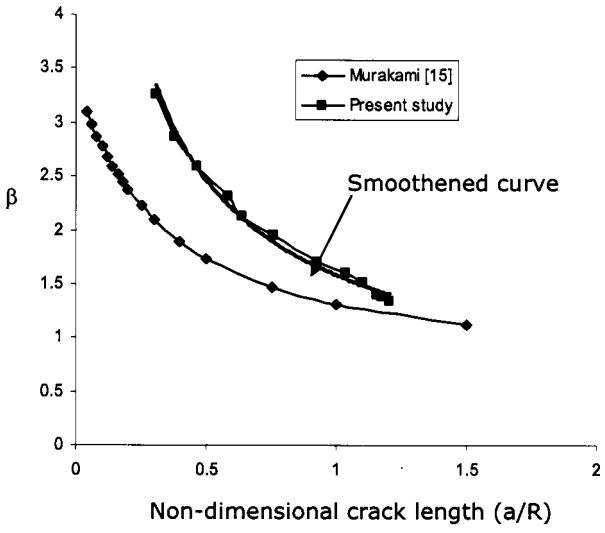

Fig.13 Plot of geometry factor variation

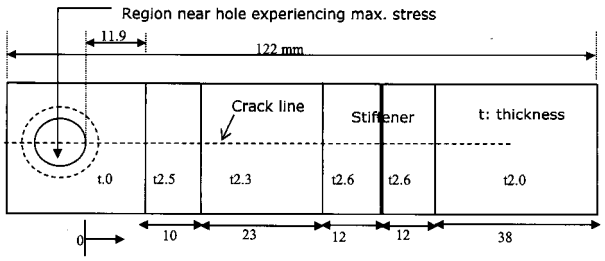

Fig. 14 Geometry details of the region chosen for refinement

Figure 13 shows the variation of geometry factor (β) with non-dimensional crack length. From Fig.13, it is observed that the β factor variation trend is similar to those values of Murakami (1987). However, the values differ by about 25%. The difference in the values can be attributed to approximation of geometry and eccentricity of loads. The sudden change in β factor values at selected locations is due to the variation in thickness. This validates the FE model and the procedure adopted for computation of SIF for an integrally stiffened WBSP.

As mentioned earlier the maximum tensile stress (σ_x) for WBSP with stiffeners occurs at one of the auxiliary holes, around the cut-out. This location is indicated in Fig. 9. It is assumed that another symmetrical crack is not present at the other side of the cut-out.

Figure 14 shows the geometry details of the area chosen for refinement. Fig. 15 shows the refined FE Model

Table-3 : Crack length Vs SIF

Crack length, mm	SIF, MPa$\sqrt{m}$	
	Displacement extrapolation technique	SERR technique
2.95	8.03	
6.95	11.49	11.4
7.95	11.82	
11.95	14.34	
17.95	14.69	14.27
18.95	14.85	
21.95	16.02	
28.95	16.36	16.31
29.95	16.46	
37.95	17.11	16.76
38.95	17.16	
44.95	16.25	
48.95	16.76	
51.95	17.21	16.88
52.95	16.84	
54.95	16.41	15.94
55.95	15.64	
57.1	5.77	
57.25	7.91	
57.95	9.07	9.46
58.95	9.13	
59.95	9.19	
62.987	9.62	9.17
64	9.69	
68.95	11.79	

including zoomed view of a narrow strip in WBSP encompassing the crack path. It also gives the salient details of the FE mesh used for analysis. Cracks of different length from the hole towards the stiffener are modelled by separating the finite elements at the nodal points along the crack line. Crack tip singular elements are generated in order to compute SIF accurately. SIF is computed for every small increment of crack length. Under the integral stiffener, it is assumed that the crack is propagating in the plate and the remaining depth of the stiffener is uncracked. FE modelling is carried out for different crack lengths to

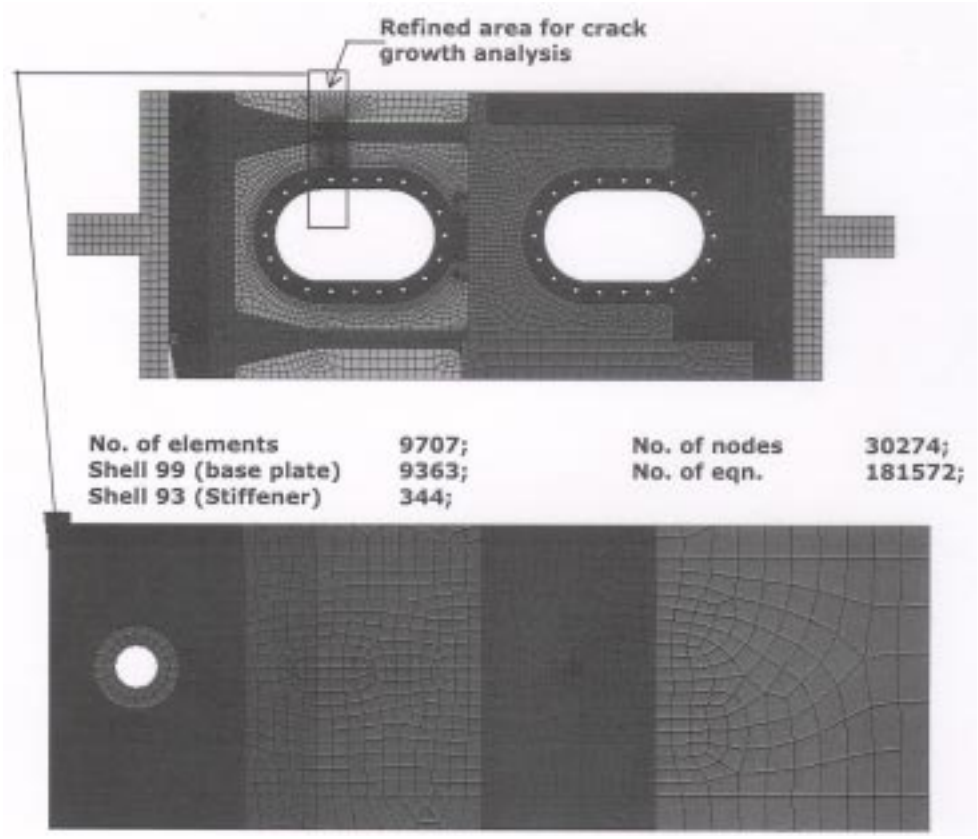

Fig. 15 Refined FE model with zoomed view

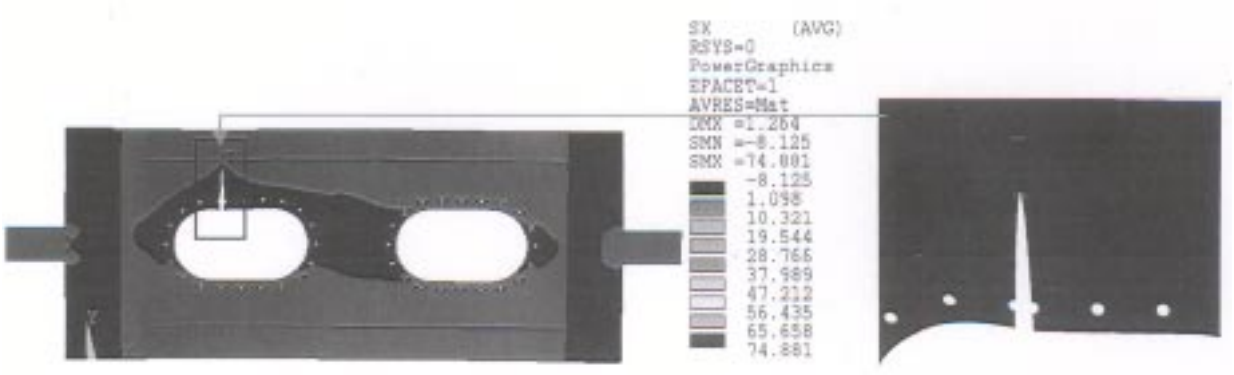

Fig. 16(a) σ_x - stress contour

Fig. 16(b) Zoomed view of deformed crack

compute SIF under a remotely applied load of 20 kN and appropriate boundary conditions. SIF for mode I is computed by using displacement extrapolation technique. A plot of stress (σ_x) contour and crack propagation is shown in Figs. 16(a) and 16(b) respectively. Table-3 shows the SIF values for different crack lengths. Fig. 17 shows the plot of SIF variation with crack length. It can be seen from Fig. 17 that SIF increases with crack length as it approaches the stiffener and then begins to drop even though crack propagates further. The stiffener alters the stress distribution near the crack tip and offers resistance to crack propagation. The opening mode SIF is less for the crack tip in the vicinity of an intact stiffener because the load is taken by the stiffener and the stress is lowered in the plate. SIF reaches a minimum value just after the stiffener location and then begins to increase again with crack length. For some of the selected crack lengths, SIF is calculated using SERR technique [16] and the values are also shown

in Table-3. It is observed from Table-3 that SIF values calculated using SERR technique are found to be in good agreement with those of obtained using displacement extrapolation technique.

As already mentioned that under extreme loading conditions, the stiffener may break. In view of this, studies are also carried out to compute SIF for broken stiffener condition. SIF for an unstiffened WBSP panel is also calculated to illustrate the effect of broken- stiffener and intact-stiffener conditions. Fig. 17 shows the variation of SIF for intact-stiffener, broken-stiffener and unstiffened conditions. It is observed from the plot that in the case of broken-stiffener condition, there is significant increase of SIF for the crack tip just after the stiffener location. This value is even higher than that of the unstiffened case. This may be due to the eccentricity of the load and the additional energy release due to breaking of the stiffener. In all the cases, it is observed that the computed SIF values are less than the fracture toughness of the material 2024-T3 Al alloy. It is clearly observed from SIF plots of intact-stiffener and unstiffened condition that the effect of stiffener on SIF is less when the crack tip is away from the stiffener and gradually increases when the crack reaches the stiffener.

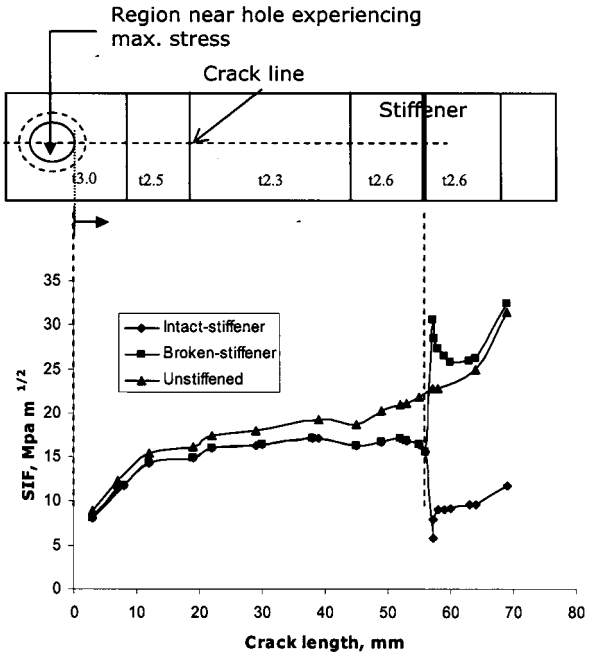

Fig. 17 Plot of SIF variation for different stiffener conditions

Damage Tolerance Evaluation

As already mentioned, this aircraft has been designed complying with the Federal Aviation Regulations (FAR-25) [17]. Section 25.571 of FAR-25 is concerned with the damage tolerance evaluation of an aircraft. Section 25.571 requires that evaluation of the structural strength, detailed design and fabrication must show that catastrophic failure due to fatigue, corrosion or accidental damage, will be avoided throughout the operational life of the aircraft. To meet this requirement, each part/component of the aircraft structure should be evaluated against fatigue failure and fracture. As a step towards realisation of this critical requirement, damage tolerance evaluation of WBSP is carried out by examining the residual strength of this critical component. The extent of damage for residual strength evaluation at any time within operational life must be consistent with the initial crack/defect detectability and its subsequent growth under repeated loads. The existence of a crack in a structure will result in lowering the residual strength of the structure below the ultimate strength of the material. The amount of strength that is left in a structure after crack initiation, which is supposed to withstand the service load (P_s) throughout its design life, is called the residual strength. The remaining strength under the presence of cracks is generally referred to as the 'residual strength', P_{res}. With a residual strength $P_{res} < P_u$, the safety factor, (j) decreases. That is,

$$j = \frac{P_{res}}{P_s} < \frac{P_u}{P_s} \tag{8}$$

where

P_u = ultimate strength of the structure without defect

P_s = service load

It is known that damage tolerance analysis provides both residual strength diagram and crack growth curve. Present study is limited to evaluation of residual strength. Residual strength can be computed by using (i) plastic collapse condition and (ii) fracture toughness criterion. The residual strength of a plate panel is the least value obtained by following the above two criteria.

Plastic Collapse Condition [18]

In the plane stress condition where the stress in the entire cross section is equal to yield strength at the time of collapse, the maximum load carrying (P_{max}) capacity of the plate with an edge crack is

$$P_{\max} = t(W - a)\,\sigma_y \tag{9}$$

where, a = crack length, W = total width, t = thickness, and σ_y = yield strength

This failure load is called the collapse load or the limit load.

The nominal stress in full width of the component is,

$$\sigma = \frac{P_{\max}}{Wt} \tag{10}$$

Hence the component fails when the nominal stress is

$$\sigma_{fc} = \frac{P_{\max}}{Wt} = \frac{t(W-a)\,\sigma_y}{Wt} \tag{11}$$

If a = W, failure will occur when the nominal stress $\sigma_{fc} = 0$

Fracture Toughness Criterion [18]

The nominal stress at which fracture takes place, will be denoted as σ_{fc}

$$\sigma_{fc} = \frac{\text{Fracture toughness}}{\beta\sqrt{\pi a}} \tag{12}$$

where, σ_{fc} is the residual strength or the remaining strength under the presence of cracks

The residual strength of WBSP is calculated using the following data.

In-plane tensile load = 20 kN
Width of the panel = 360 mm
Average thickness = 2.5 mm
Fracture toughness = 36.27 MPa $m^{1/2}$
Yield strength = 365 MPa
Average stress, σ_{avg} = 22.2 Mpa

Using eqns. (9) to (12) and the values of Table-3, the residual strength is computed based on plastic collapse condition and fracture toughness criterion. Table-4 shows the residual strength values obtained by using the two methods described above. From Table-4, it is observed that the values obtained by fracture toughness criterion are less compared to those obtained by using plastic collapse condition. Hence, the residual strength values corresponding to fracture toughness criterion are considered for damage tolerance evaluation. The corresponding residual strength diagram for the intact-stiffener is shown in Fig.18. Residual strength is also calculated for the plate with broken-stiffener and no-stiffener conditions. Fig.18 also shows the variation of residual strength with crack length for broken stiffener and unstiffened conditions. Point 1 identified in Fig. 18 which is the minimum value indicates the residual strength of the panel. If the stiffener remains intact when the crack tip reaches the stiffener, the stiffener can arrest the crack up to a design stress of 1397MPa which is about 300% higher compared to the unstiffened condition. From Fig. 18, it is observed that in the case of broken-stiffener condition, the residual strength for the crack tip just after the stiffener location

Table-4 : Crack length Vs Residual strength

Crack length, mm	Residual strength (MPa) by	
	Fracture toughness criterion	Plastic collapse criterion
2.95	1003.9	3613.5
6.95	701.4	3554
7.95	682	3539
11.95	562.1	3479.9
17.95	548.8	3405
18.95	542.9	3393.4
21.95	503.37	3356.3
28.95	492.7	3276.7
29.95	489.8	3265.3
37.95	471.27	3174.3
38.95	469.61	3162.9
44,95	495.9	3094.7
48.95	480.9	3043.2
51.95	468.3	3004.6
52.95	478.6	2991.8
55.95	515.5	2953.2
57.1	1397	2940.8
57.25	1020	2936.5
57.95	889.2	2927.5
59.95	877.4	2901.8
62.987	838.8	2862.7
64	831.69	2849.7
68.95	683.6	2786.1

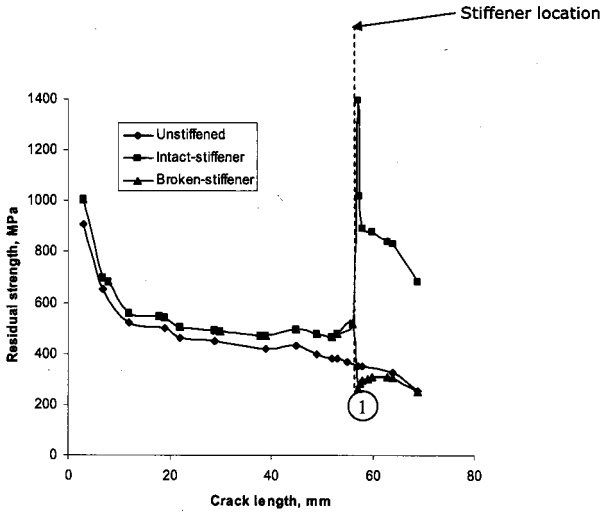

Fig. 18 Plot of variation of residual strength for different stiffener conditions

decreases by about 80% compared to the intact-stiffener condition and by 25% compared to the case of unstiffened condition. It is also observed that the residual strength for all the crack lengths under intact-stiffener condition is higher than those of the values computed under unstiffened condition.

Summary

Methodologies for damage tolerance evaluation of one WBSP of an aircraft have been presented. Static analysis of WBSP has been conducted by using FEM. It is observed that maximum tensile stress (σ_x) occurs at one of the auxiliary holes, around the cut-out. Static test was conducted on WBSP for the same loading condition. Static analysis results obtained by FEA and experiment were compared at critical locations and it is observed that there is good agreement between them. Fatigue crack has been modelled at the point of maximum stress location towards the cut-out free surface and later towards the integral stiffener. SIF for different crack lengths for mode I is computed by using displacement extrapolation technique and for some selected crack lengths SIF is calculated by using SERR technique and the values were compared. It is observed from SIF plot that under intact-stiffener condition, SIF increases for certain crack length and then begins to drop as the crack tip approaches the intact-stiffener. The stiffener alters the stress distribution near the crack tip and offers resistance to crack propagation. The opening mode SIF for the crack tip is less in the vicinity of an intact-stiffener because the load is taken by the stiffener thereby the stress is lowered in the plate. SIF reaches a minimum value just after the stiffener location and then begins to increase again with crack length. For damage tolerance evaluation, residual strength is calculated by making use of computed SIF values. From residual strength plot, it is observed that the stiffener can arrest the crack up to a considerable amount of design stress. Residual strength is also calculated for WBSP under broken-stiffener and unstiffened conditions. Significant difference in residual strength has been observed with respect to intact stiffener and broken stiffener conditions when the crack reaches the stiffener location. This may be attributed to additional release of energy due to the breaking of stiffener.

Acknowledgements

We acknowledge with thanks the sponsors National Aerospace Laboratories (NAL), Bangalore for funding the project. We also thank Dr. P.K. Dash and Dr. Yegna Narayanan, NAL, for their technical help and suggestions. We acknowledge with thanks the valuable technical suggestions and support provided by our colleague Mr. S. Bhaskar, Scientist during the course of this investigation. We are grateful to our colleagues Mr. T. Narayanan, Head, EML, Dr. K. Ravisankar and his team members, EML, for sharing the static analysis experimental results of WBSP. This paper is being published with the permission of the Director, SERC, Chennai, India.

References

1. Rooke, D.P. and Cartwright, D.J., "Compendium of Stress Intensity Factors", HMSO, London, 1976.

2. Viegler, H., "The Residual Strength Characteristics of Stiffened Panels Containing Fatigue Cracks", Engg. Fract. Mech., Vol. 5, pp. 447-477, 1973.

3. Shakarayev, S.V. and Moyer, E.T., "Edge Cracks in Stiffened Plates", Engg. Fract. Mech., Vol. 27, pp. 127-134, 1987.

4. Toor M. Pir., "A Review of Some Damage Tolerance Design Approaches for Aircraft Structures", Engg. Fract. Mech., Vol. 5, No.4, pp. 837-876, 1973.

5. Wood A. Howard., "Application of Fracture Mechanics to Aircraft Structural Safety", Engg. Fract. Mech., Vol. 7, No.3, pp. 557-558, 1975.

6. Brussat, T.R., Kathiresan, K. and Rudd, J.L., "Damage Tolerance Assessment of Aircraft Attachment

Lugs", Engg. Fract. Mech., Vol. 23, No. 6, pp. 1067-1084, 1986.

7. Toor M. Pir. and Double Dagger., "On Damage Tolerance Design of Fuselage Structure (Circumferential Cracks)", Engg. Fract. Mech., Vol. 26, No.5, pp. 771-782, 1987.

8. Toor M. Pir. and Double Dagger., "On Damage Tolerance Design of Fuselage Structure (Longitudinal Cracks)", Engg. Fract. Mech., Vol. 24, No.6, pp. 915-927, 1986.

9. Swift, T., "Fracture Analysis of Stiffened structure. Damage Tolerance of Metallic Structures", Analysis Methods and Application, ASTM STP842, pp. 69-107, 1984.

10. Roudolff Florence. and Michael Gadre., "Damage Tolerance of Composite Structures for Large Transport Aircraft", Aerospace Science and Technology, Vol. 4, No.1, pp. 23-32, 2002.

11. Zienkiewicz, O.C. and Taylor, R.L., The Finite Element Method-Vol.I. The basics Vol.II, Solid Mechanics, Butterworth-Hieneman Limited, 2000.

12. ANSYS 6.0, Theory and Reference Manual, 2002.

13. Rama Chandra Murthy, A., Rajasankar, J., Palani, G.S., Nagesh R. Iyer., Bhaskar, S. and Girish, K.E., "Crack Growth Study of Wing Bottom Skin Panel using ANSYS", ANSYS India User Conference, Bangalore, India, 2002.

14. Irwin, G.R., "Analysis of Stresses and Strains Near the End of a Crack Traversing a Plate", Journal of Applied Mechanics, Vol. 24, 1957.

15. Murakami, Y., Stress Intensity Factors-Handbook, Pergamon Press, 1987.

16. Anderson, T.L., Fracture Mechanics: Fundamentals and Applications, CRC Press, 1995.

17. Federal Aviation Regulation (FAR) Part 25 - Airworthiness Standards. Transport Category Airplanes,

18. Broek David., The Practical Use of Fracture Mechanics, Kluwer Academic Publishers, 1989.